Climate Dynamics (2022) 58:1403–1418
https://doi.org/10.1007/s00382-021-05967-7

Multidecadal seesaw in cold wave frequency between central Eurasia and Greenland and its relation to the Atlantic Multidecadal Oscillation

Yusen Liu[1] · Cheng Sun[1] · Zhanqiu Gong[1] · Jianping Li[2,3] · Zhen Shi[4]

Received: 4 June 2021 / Accepted: 13 September 2021 / Published online: 30 September 2021

Abstract
During the winter, the cold wave activity over the mid-high latitudes has profound impacts on agriculture, economic and human wellbeing. Such extreme weather events have been connected with the East Asia winter monsoon system and significantly influence the climate over the Eurasian continent. However, the multidecadal variabilities and regional interconnections of the cold wave activity across the Northern Hemisphere are lesser-known. In this study, we investigate the multidecadal variations in the cold wave frequency (CWF) and find an inverse relationship between Greenland and central Eurasia. Observational and modeling evidence suggests that the Atlantic Multidecadal Oscillation (AMO) is likely to be the driving force of the multidecadal seesaw in CWF, while the effects of the Arctic sea ice are very limited. The increased sea surface temperature (SST) in association with the AMO warms the subpolar troposphere and weakens the predominant westerlies over mid-high latitudes, resulting in positive geopotential height anomalies over the subpolar region. This further weakens the Icelandic Low and strengthens the Siberian High, which directly induces the warming (cooling) over Greenland (central Eurasia). There is a strong coherence between the mean state of surface air temperature and temperature extremes. The AMO-induced warming/cooling in Greenland/central Eurasia corresponds well with less/more frequent cold wave activities. Our results provide new insight into the multidecadal variability of cold wave activities and suggest that the CWF in the Northern Hemisphere may be interlinked.

Keywords Cold wave frequency · Multidecadal variability · Atlantic Multidecadal Oscillation · Atmospheric circulation

1 Introduction

Frequent cold weather extremes during the boreal winter, such as cold waves (CWs), snowstorms, and freezing rain, tend to be increasing in the Eurasian continent recently (Cohen et al. 2012; Liu et al. 2012; Mori et al. 2014). For example, changes in the average winter air temperatures in East Asia can be attributed directly to the East Asian winter monsoon (Wang et al. 2009; Wang and Chen 2014). The sea-land thermal difference is an essential driver of the winter monsoon since the continental radiative cooling effect is much stronger in the land than in the ocean. The cold waves in Eurasia often correspond to enhanced Siberian High, which leads to an intensified winter monsoon. Thus, an increase of cold wave frequency (CWF) in Eurasia can be a source of increased cold extremes during winter in East Asia (Gong et al. 2001; Wu and Wang 2002a, b; Wu et al. 2009; Jiang et al. 2013; Jia et al. 2017).

The thermal conditions in Eurasia exhibit a prominent interdecadal variability, with a significant cooling trend since the 1990 s and persist till the 2010 s (over − 1 °C/decade) under the circumstances of increased greenhouse gases (Li et al. 2015; Sun et al. 2016b). Some studies have linked this phenomenon to the global warming hiatus during 1998–2013 (Cohen et al. 2012; Huang et al. 2017b; Li et al. 2015). The global warming signal may be partially

✉ Cheng Sun
scheng@bnu.edu.cn

1 College of Global Change and Earth System Science (GCESS), Beijing Normal University, Beijing 100875, China

2 Key Laboratory of Physical Oceanography, Frontiers Science Center for Deep Ocean Multispheres and Earth System (FDOMES), Institute for Advanced Ocean Studies, Ocean University of China, Qingdao 266100, China

3 Laboratory for Ocean Dynamics and Climate, Pilot Qingdao National Laboratory for Marine Science and Technology, Qingdao 266237, China

4 National Marine Environmental Forecasting Center, Ministry of Natural Resources, Beijing, China

offset by the decreasing trend in land surface air temperature, especially over the Eurasian continent. This suggests that the greenhouse effect cannot explain the observed temperature changes in Eurasia. The cold wave activities are witnessed to increase and hit Eurasia more often, corresponding to a colder Eurasian winter during the recent decades, consequently resulting in considerable social and economic losses.

The causes of changes in the Eurasian CWF have not reached a consensus (Gao et al. 2015). Various studies have pointed out that the reduction of Arctic sea ice and the accompanying variations of middle- and high-latitude atmospheric circulations during the same period are responsible for the increased Eurasian CWF (Honda et al. 2009; Kug et al. 2015). In recent decades, the trends in winter surface air temperature at middle and high latitudes in the Northern Hemisphere are significantly correlated with the Arctic sea ice loss, especially in the Barents-Kara Sea region (Li et al. 2019b). There is a positive feedback between the Arctic sea ice decline and rapid local air temperature warming, which involves changes in ice albedo, polar cloud and water vapor content, and radiative fluxes (Francis and Vavrus 2015; Screen and Simmonds 2010; Serreze and Barry 2011). Some studies suggested that sea ice reduction and its related warming amplification in the Arctic reduce the meridional temperature gradients in the lower troposphere. As a result, the mid-latitude westerly jet stream weakens, and the propagation speed of large-scale Rossby waves is reduced. This further increases the intensity, frequency, and persistence of the atmospheric blocking activity. The incursions of cold air masses from the Arctic into mid-latitudes of Eurasia continents are also enhanced, leading to increased CWF in Eurasia (Francis and Vavrus 2015).

However, the impact of Arctic sea ice decline on Eurasian wintertime air temperature remains uncertain. Several studies have shown that changes in atmospheric circulation at middle latitudes lead to the Arctic sea ice reduction. For example, the temperature cooling and CW activities in Eurasia lead the Arctic sea ice reduction by about 1–2 months. This suggests that increased Eurasian CWs are unlikely caused by the Arctic sea ice decline but are driven by mid-high latitudes atmospheric circulation variability, which may also lead to the Arctic sea ice melting (Kelleher and Screen 2018; Sun et al. 2016c). Recent studies have shown that the driving effect of atmospheric circulation variability at mid-high latitudes on the Arctic sea ice loss is significant (Ding et al. 2019). The contributions of heat and water vapor transport from Eurasia to the Arctic are critical in the Arctic warming amplification phenomenon (Screen et al. 2012). Various studies suggest a weak impact of the Arctic sea ice decline on Eurasia CW activities based on model results. There is also modeling evidence showing no reliable link between Arctic sea ice decline and Eurasian CWF increase (Mori et al. 2014; Screen 2017). No significant evidence shows that the frequency and intensity of the CWs are intensified in association with the reduction of Arctic sea ice in the observational data (Barnes et al. 2014). Therefore, the Arctic sea ice variability may not be the only driving force affecting the variations of CWF in Eurasia.

The Eurasian winter climate may also be modulated by multiple factors due to its own complexity and the active interactions among other components of the Earth system. Previous studies demonstrated relationships between the Eurasian winter climate and tropical/subtropical sea surface temperatures (SST) (Luo et al. 2017; Sun et al. 2015, 2016a, 2017b; Zhao et al. 2016), which have also been linked to the Arctic sea ice loss (Jung et al. 2017; Li et al. 2018; Perlwitz et al. 2015; Tokinaga et al. 2017). The role of the Atlantic SST multidecadal variability in Eurasian climate change is also emphasized (Li et al. 2019a; O'Reilly et al. 2017; Sun et al. 2015, 2017b; Wang et al. 2019). As one of the most well-known global SST variability patterns at multidecadal timescales, the Atlantic Multidecadal Oscillation (AMO; Kerr 2000) is recognized to have profound climate effects. It affects the climate not only around the Atlantic region (Enfield et al. 2001; McCabe et al. 2004; Sutton and Dong 2012; Sutton and Hodson 2005) but also the remote regions (Li and Bates 2007; Lu et al. 2006; Sun et al. 2015, 2017b). Additionally, the AMO contributes to the out-of-phase decadal climate pattern (Sutton and Hodson 2005; Feng et al. 2011). However, most studies on the AMO climatic impacts are based on the averages of temperature and precipitation, while its effects on the variations of cold extremes and CW activity at decadal time scales are little known. Meanwhile, several recent studies on winter surface air temperature variability over mid-high latitude NH have focused on either the zonal mean temperature changes (Screen 2014; Cohen 2016) or a specific region, like North America, and so on (Zhang et al. 2012; Mori et al. 2014; Rhines et al. 2017). Yu and Lin (2018) pointed out that the wintertime surface air temperatures over North Asia and North America co-vary at interdecadal time scales, which is linked by extratropical teleconnection patterns. However, the co-variability of CWF in Eurasia and other regions is still unknown (Chen et al. 2019).

In this study, by using the observational data, we find the multidecadal variabilities of CWF over Eurasia and Greenland are highly anticorrelated, forming a seesaw pattern in the CW activity. We also examine the correlations between the cold wave frequency and multidecadal climate variability (i.e., AMO) based on the observations/reanalysis and model simulations. We also attempt to explain how the multidecadal SST variability modulates the CWF seesaw between Eurasia and Greenland. This may also have implications for better understanding the decadal variability and predictability of cold-related extreme events over these two regions.

2 Data and methodology

2.1 Cold wave frequency

Cold waves have various definitions. Cold events can be defined as a number of consecutive days when the minimum air temperature (TN) values below a certain threshold. Some studies have recently developed excess cold factor (ECF) to better analyze extreme cold events (Nairn and Fawcett 2013; Wang et al. 2016). The ECF considers the cumulative effect of maximum air temperature (TX) and TN in a 3-day period contrasted with a prior 30-day acclimation period to quantify the intensity of a cold event. The acclimatization period used in the ECF considers a wide range of physiological adaptation processes (Scalley et al. 2015) that may result in human body responses to CWs. This method can be used as a better indicator for measuring CWs, and it can be used in more various climatic conditions compared with that only based on daily values of TN (Nairn and Fawcett 2013, 2015).

Following Piticar et al. (2018), cold waves (CWs) are measured by the ECF in this study and calculated based on percentile values. The calculation of the ECF contains two excess cold sub-indices incorporating both TX and TN. Two excess cold sub-indices are given by the following:

$$ECI_{sig} = \left[\left(Tm_i + Tm_{i-1} + Tm_{i-2}\right)/3\right] - Tm10i \quad (1)$$

$$ECI_{accl} = \left[\left(Tm_i + Tm_{i-1} + Tm_{i-2}\right)/3\right]\left[-\left(Tm_{i-3} + \cdots + Tm_{i-32}\right)/30\right] \quad (2)$$

where Tm_i is the daily mean temperature of day i (Tm is the average of TX and TN of the same day i as Tm = (TX + TN)/2)) and Tm10i is the 10th percentile of Tm calculated for each calendar day (day i) of the extended winter (November–March).ECI_{accl} is the excess cold index for acclimatization and measures cold stress induced by short-term temperature contrast, while ECI_{sig}sub-index refers to a significant excess cold against long-term climatic conditions. In terms of air temperature, the ECI_{accl} sub-index assesses the human body's acclimatization to its local climate in 30 days.

Then the ECF is expressed as the following:

$$ECF = -ECI_{sig} \times min\left(-1, ECI_{accl}\right) \quad (3)$$

The negative values of ECF indicate CW conditions, and a CW event is defined as a period of at least three consecutive days. Calculations of CW indices require at least three consecutive days, and this is derived from studies on human responses to the onset of extremely cold weather, as a significant rise in the mortality rate above its antecedent rate in cold weather takes at least three consecutive days (Nairn and Fawcett 2015; Wang et al. 2016).

We also employ Cold Wave Frequency (CWF) index to assess changes in CWs in this study. It is defined as the annual number of days that contribute to CWs as identified by the annual number of individual CWs calculated based on ECF that occur in each extended wintertime (November–March).

2.2 Data and index definitions

As we mainly focus on the cold waves in this study, the following data we used are all based on the extended winter season (November–March).

The surface air temperatures used in calculating the CWF index are derived from the Berkeley Earth Surface Temperature Project data set (Rohde and Hausfather 2020) for the period 1900–2019 and HadGHCND data set (Caesar et al. 2006) from 1950 to 2014.

The global observational sea surface temperature (SST) data set used in this study is the Extended Reconstruction SST version 3 (ERSST v3b) data set (Smith et al. 2008) and ERSSTv5 data (Huang et al. 2017a) for the period 1900–2019. Atmospheric data sets are derived from the NOAA ESRL Twentieth Century Reanalysis, version 2 (20CRv2) data set (Compo et al. 2011), for the period 1900–2013 and observational data of the surface air temperatures are derived from Climatic Research Unit (CRU) data set (Harris et al. 2013) for the period 1900–2019. The Pan-Arctic Ice Ocean Modeling and Assimilation System (PIOMAS and PIOMAS-20 C) reconstructions of monthly Arctic sea ice volume over the period of 1901–2010 are used to characterize the multidecadal variations of the Arctic sea ice, and the dataset can be downloaded from the following link http://psc.apl.uw.edu/research/projects/piomas-20c/ (Schweiger et al. 2019).

The AMO index is defined as the area-weighted average of SST anomalies over the North Atlantic region (0°–60° N, 80° W–0°), similar to that defined by Enfield et al. (2001). And the index used in this study comes from the NOAA ESRL Climate Timeseries, which is calculated based on the ERSST data set (Smith et al. 2008). The decadal component of the AMO is derived from an 11-year running mean, and the long-term trend is removed to isolate the multidecadal variability. The Pacific Decadal Oscillation (PDO) Index is defined as the leading principal component of North Pacific monthly sea surface temperature variability (poleward of 20° N) (Mantua et al. 1997).

2.3 Statistical methods

A two-tailed Student's t-test is used to determine the statistical significance of the linear regression and correlation between two autocorrelated time series. We use the effective

number of degrees of freedom, N^{eff}, which is given by the following approximation:

$$\frac{1}{N^{eff}} \approx \frac{1}{N} + \frac{2}{N}\sum_{j=1}^{N}\frac{N-j}{N}\rho_{XX}(j)\rho_{YY}(j) \quad (4)$$

where N is the sample size, and $\rho_{XX}(j)$ and $\rho_{YY}(j)$ are the autocorrelations of two sampled time series X and Y, respectively, at time lag j (Li et al. 2013; Sun et al. 2015).

The CWF linear trends expressed in this study for both datasets are calculated using a nonparametric estimation technique based on Sen's slope estimator (Sen 1968). This method is a robust estimation of the linear trends as it makes no assumption about the distribution for the residuals. Sen's slope method is much less sensitive to the effect of outliers in the time series than the least-squares method. It has been widely used in studies of the effects of climate change on hydrology and climate extremes (Sun et al. 2019; Zhao et al. 2016). The statistical significance of Sen's slope is tested by the nonparametric Mann-Kendall method (Zhao et al. 2016).

2.4 AGCM experiments

A series of atmospheric general circulation model (AGCM) experiments are employed in this study to investigate the atmospheric circulation response to a specific SST pattern. The AGCM model is referred to as primitivE-Equation DYnamics (SPEEDY) model developed at the Abdus Salam International Centre for Theoretical Physics (Kucharski et al. 2013), which is based on a spectral primitive-equation dynamical core. SPEEDY is an intermediate AGCM that contains eight vertical levels with a horizontal resolution of T30 (3.75° × 3.75° grid). It is hydrostatic, and sigma-coordinates and semi-implicit treatment of gravity waves are used.

We conducted AGCM experiments forced by SST variations in the North Atlantic Ocean. To isolate the impact of the North Atlantic SST forcing, we run the AGCM forced by raw observed monthly-varying SSTs prescribed over the North Atlantic basin (0° –60° N, 80° W–10° E). Climatological mean monthly SSTs are prescribed in other basins outside the North Atlantic to highlight the direct impacts of the North Atlantic SST variability on the Northern Hemisphere atmospheric circulation. This experiment is referred to as NA_EXP. The model integrations start in 1880 and run through 2013. An ensemble of five members is generated by restarting the model using small initial perturbations. The first 20 years of all simulations are considered to be a spin-up time for simulation, and the analysis is performed on the remaining period from 1900 to 2013. The NA_EXP experiment is transient runs, and the results of the ensemble members from the experiment were averaged and analyzed for the period 1900–2013. The simulated responses to the AMO SST forcing are defined as the composite differences between the AMO warm and cold phases to examine the impacts on the atmospheric circulation during the boreal winter.

3 Results

3.1 Seesaw in cold wave frequency between central Eurasia and Greenland at decadal time scales

Figure 1 shows the trend of cold wave frequency (CWF) over the Northern Hemisphere derived from two different data sets since 1990. Both datasets exhibit opposite signs of a long-term trend in CWF, with a strong decreasing trend over Greenland (60°–75° N, 60°–45° W) and a significant increasing trend over central Eurasia (40°–55° N, 75°–100° E). The trend patterns of CWF correspond with the winter-time surface air temperature, as suggested in the previous studies. The cold wave frequency is closely related to the surface air temperature cooling (warming) when there are more (fewer) CWs. The decline of CWF over Greenland is consistent with the recent warming trend (Ding et al. 2014), while more frequent CW activities correspond well with the cooling over central Eurasia (Screen et al. 2015; Sigmond and Fyfe 2016), which is caused by the changes in atmospheric backgrounds (Horton et al. 2015). However, few studies focus on the reversed tendencies of CWF between central Eurasia and Greenland but mainly focusing on individual regions (e.g., North America and Eurasia). Our results indicate the contrasting long-term trends in CWF between Greenland and central Eurasia, further implying a potential linkage may exist.

Figure 2 shows the time series of the CWF index (defined by the area-averaged CWF). It suggests that the CWF in central Eurasia exhibits the opposite phase to that in Greenland and the decadal variabilities are significant in both data sets (Fig. 2). The correlation coefficients of the CWF between central Eurasia and Greenland at decadal time scales reach − 0.70 for the period 1900–2019 from the Berkeley data set (Fig. 2a) and − 0.72 for the period 1950–2014 from the HadGHCND data set (Fig. 2b). The CWF in the two regions consistently exhibits three phase shifts around 1920, 1980, and 2000 for the period 1900–2019 using the Berkeley data. Also, the recent two phase shifts are well captured by the HadGHCND data, consistent with the Berkeley data. This supports the high coherence of CWF in central Eurasia and Greenland. The central Eurasia CWF is low before 1915, as the CWF is well below 20d on both interannual and interdecadal time scales. More frequent CW activities are observed for the period 1920–1980 in central Eurasia, while the CWF in Greenland maintains a low phase during the same period. The CWF in central Eurasia declines significantly in

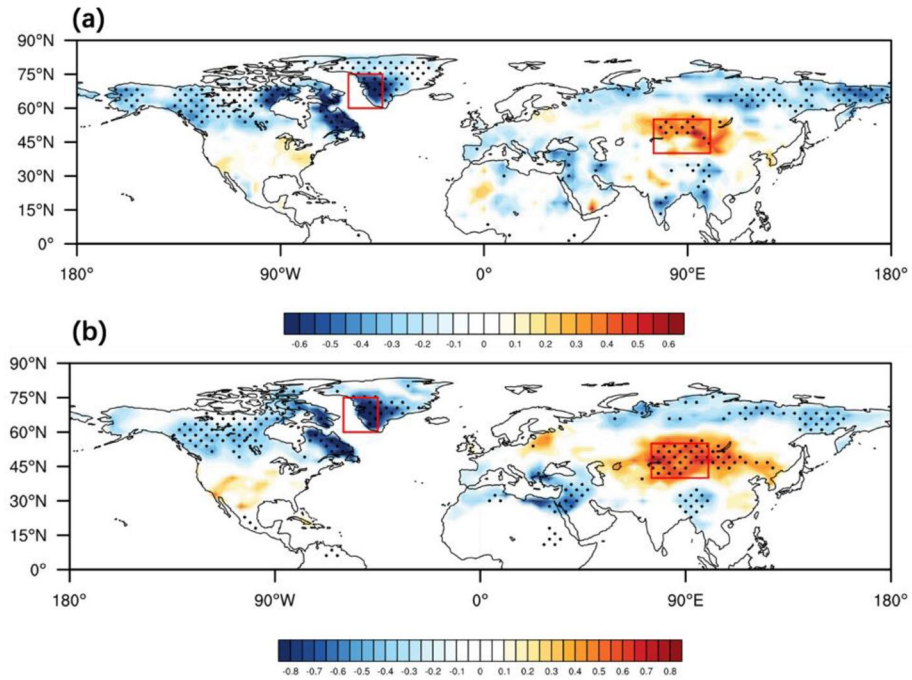

Fig. 1 The cold wave frequency trends over the Northern Hemisphere derived from **a** the Berkeley data set for the period 1990–2019 and **b** the HadGHCND data set for the period 1990–2014. Dotted shading indicates the correlation coefficients significant at the 90 % confidence level

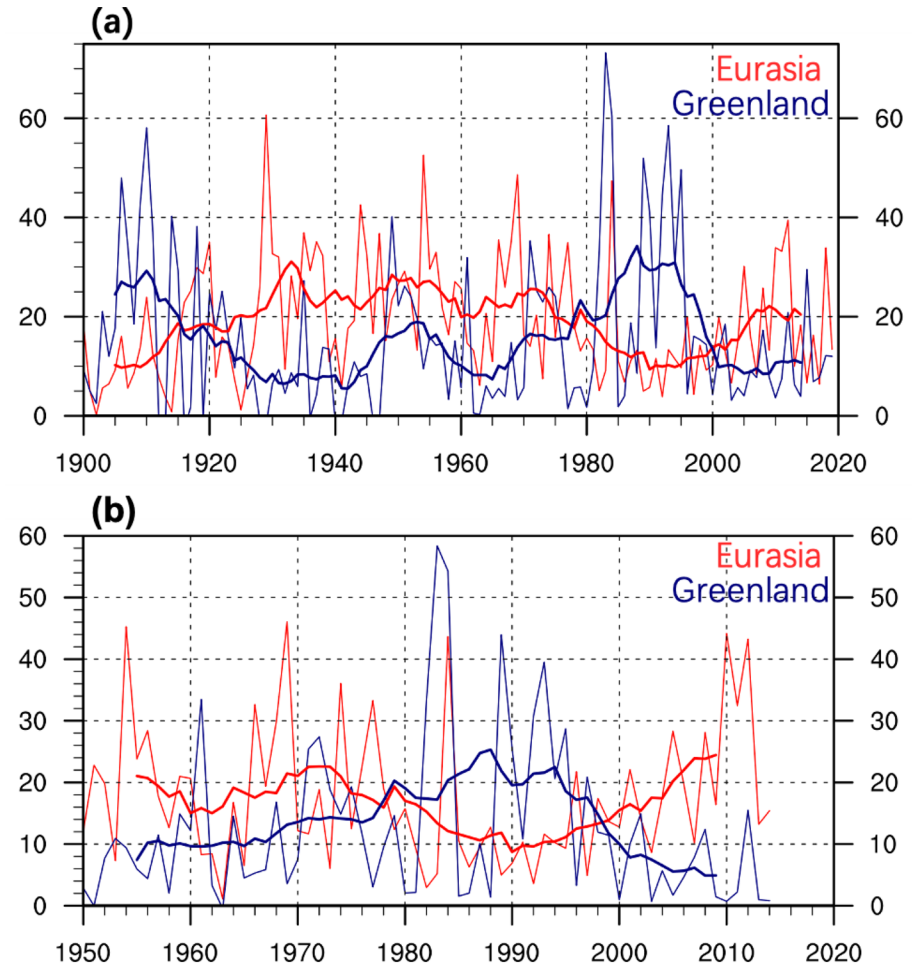

Fig. 2 Time series of the raw data (thin curves) and 11-year running averages (thick curves) of the cold wave frequency over the central Eurasia (40°–55° N and 75°–100° E; red curves; left axis in units of days) and Greenland (60°–75° N and 60°–45° W; blue curves; right axis in units of days) derived from **a** the Berkeley data set for the period 1900–2019 and **b** the HadGHCND data set for the period 1950–2014. The long-term linear trends were removed

the 1980 and 1990 s and shows a continuous increasing tendency afterward. By contrast, the CWF in Greenland increases substantially from 1965 to 1985 and declines rapidly in the recent decades. The decadal variabilities of CWF are negatively correlated between central Eurasia and Greenland, which is independent of datasets or analyzed periods. However, the interannual relationship of CWF between Eurasia and Greenland is rather weak and insignificant (−0.13 for the Berkeley data set and −0.16 for the HadGHCND data set).

The reversed relationships of CWF between central Eurasia and Greenland exist in the long-term trends (Fig. 1) as well as decadal variations (Fig. 2), but in this study, we mainly focus on the coherence on multidecadal time scales. The CWFs in these two regions are significantly correlated with opposite phases, referring to as the multidecadal seesaw. In the light of that, we define the CWF seesaw index using the CWF in central Eurasia minus that in Greenland. It indicates that the CWF seesaw index turns positive (negative) when the central Eurasian CWF is relatively stronger (weaker) than Greenland. In Fig. 3, the CWF seesaw index exhibits significant multidecadal variability, which is consistent between Berkeley and HadGHCND datasets for the period 1900–2019 and 1950–2014, respectively. The CWF seesaw index shows three phase shifts around 1920, 1980, and 2000. For the overlapping period, both datasets exhibit a consistent decreasing tendency before the 1990 s and a rapid uprising in the recent decades, corresponding to the individual variation in Fig. 2. The correlation coefficient of the CWF seesaw index from the two data sets reaches 0.93, indicating the multidecadal seesaw in CWF is robust and independent of data selection. For the latter of this study, the CWF seesaw index based on the Berkeley data set is employed in the following analysis.

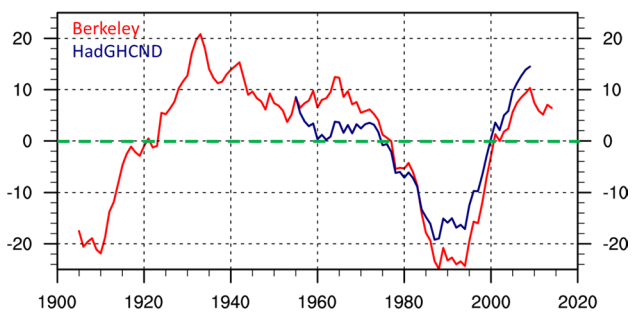

Fig. 3 Time series of cold wave frequency seesaw index with 11-year running mean derived from the Berkeley data set for the period 1900–2019 (red curve; left axis in units of days) and the HadGHCND data set for the period 1950–2014 (blue curve; right axis in units of days). The long-term linear trends were removed. The green dash line indicates zero

3.2 Relationship between AMO and cold wave frequency seesaw

Since the seesaw pattern of CWF between central Eurasia and Greenland is revealed from the above, it remains a question that which factor plays a forcing role in the CWF seesaw on multidecadal time scales. A wide range of studies indicates that the Arctic sea ice loss in recent years has profound impacts on the regional climate at mid-high latitudes (Francis and Vavrus 2012; Overland et al. 2015; Screen et al. 2013). Previous studies suggested that the recent extreme events are linked to the loss of Arctic sea ice and the associated enhanced warming (Horton et al. 2015; Ma et al. 2018; Ma and Zhu 2019). Could the changes in the Arctic sea ice dominate the co-variabilities of CWF in central Eurasia and Greenland? The observational results suggest that the relationship between the CWF seesaw and the Arctic sea ice is weak. For the spatial correlation pattern (Fig. 4a), the sea ice along the Greenland east coast shows a positive correlation, indicating the local effect of sea ice may contribute to the CW activities to some extent. However, the overall correlation map exhibits rather weak coherence over the Pan-Arctic region. The time series of the Arctic sea ice index (sea ice volume anomalies) and the CWF seesaw index barely match (Fig. 4b), as the correlation coefficient only reaches −0.17. The CWF seesaw experienced a phase shift back in the 1920 s, but no significant changes in the Arctic sea ice were observed. Overall, the CWF seesaw index and the sea ice index are negatively correlated, but it is not statistically significant. Moreover, the two series also exhibit consistent variations during the 1950 s, contrary to the overall out-of-phase relationship. Therefore, we may conclude that the time series of the Arctic sea ice and the seesaw in CWF is hardly corresponded, indicating a limited effect of the sea ice in modulating the CWF seesaw. Nevertheless, the contribution of the Arctic sea ice cannot be completely ruled out. The recent rapid sea ice melting may amplify the sea ice-reflectivity positive feedback that leads to Greenland warming (Ding et al. 2014; Outten and Esau 2012; Kug et al. 2015), further reducing the CWF in this region. Since the Arctic sea ice is unlikely to be the driving force of the CWF seesaw, other factors are needed for further inspections.

In addition, several recent studies argued that the SST variabilities are responsible for the changes of extreme climatic events in the Northern Hemisphere (Ding et al. 2014; Sigmond and Fyfe 2016; Tokinaga et al. 2017). We then inspect the correlation between the CWF seesaw index and global SSTs (Fig. 5). A positive correlation can be found over the entire North Atlantic Ocean, resembling the Atlantic Multidecadal Oscillation (AMO). This uniform warming pattern over the North Atlantic basin is consistent between different data sets and different periods. Thus, we can infer that the AMO may be connected to the

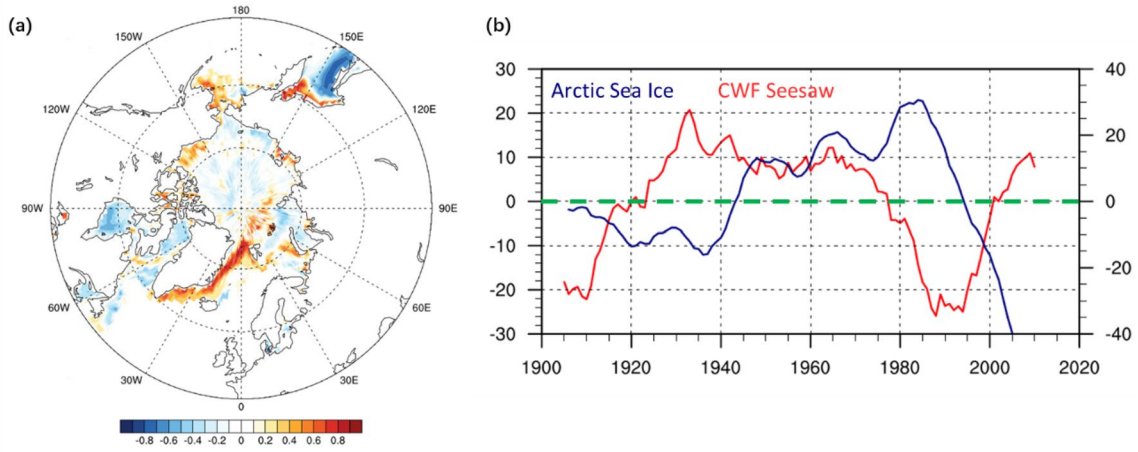

Fig. 4 **a** Correlation map between cold wave frequency seesaw index derived from the Berkeley data set and the sea ice cover for the period 1900–2019. **b** Time series of 11-year running mean cold wave frequency seesaw index (red curve; left axis in units of days) and Arctic sea ice index (blue curve; right axis in units of 10^2 km^3) for the periods 1900–2019 and 1901–2010, respectively. The long-term linear trends were removed before the analysis. The green dash line indicates zero

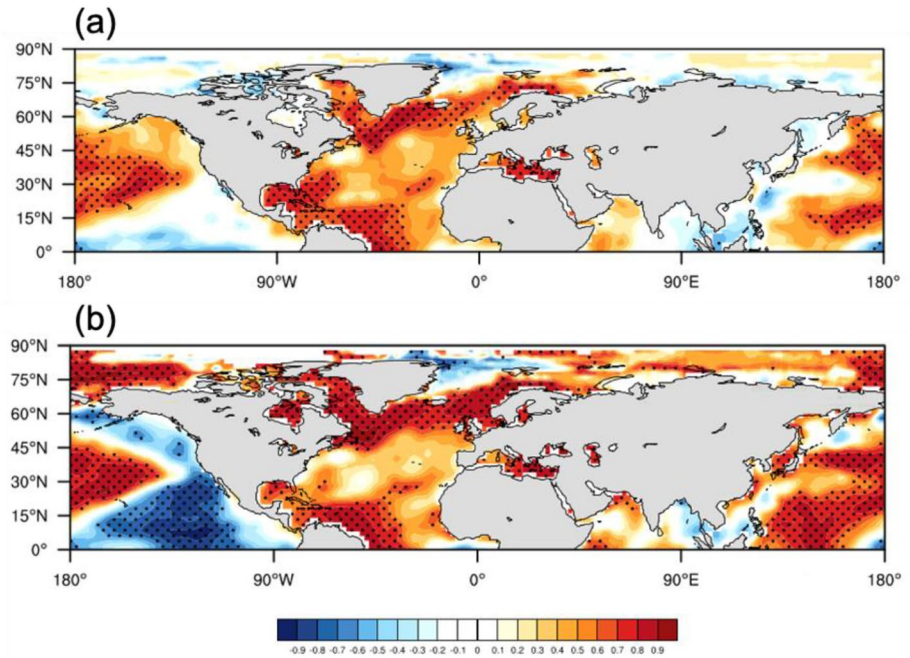

Fig. 5 Correlation maps between the decadal component of cold wave frequency seesaw index and SSTs. The CWF data are derived from **a** the Berkeley data set for the period 1900–2019 and **b** the HadGHCND data set for the period 1950–2014. The long-term linear trends were removed before the analysis. Dotted shading indicates the correlation coefficients significant at the 95 % confidence level

CWF seesaw on multidecadal time scales. Over the Pacific Ocean, the western tropical Pacific and northern North Pacific exhibit positive correlations, while the eastern North Pacific exhibits negative correlation, resembling the Pacific decadal oscillation (PDO). The two different data sets show good agreement over the North Pacific and western tropical Pacific, where the most significant SST warming can be found. This signal can be partially explained by the footprint of the remote AMO forcing, as previous studies highlighted a crucial role of AMO in the western tropical Pacific and northern North Pacific SST multidecadal variability (Sun et al. 2017a; Gong et al. 2020). However, noticeable disagreements can be found over the eastern North Pacific. For the Berkeley data, the SST cooling is relatively weak and insignificant, but for the HadGHCND data, the correlation is larger and statistically significant. This disagreement may occur largely due to the different data lengths. Nevertheless, the relationship between the CWF seesaw and the eastern North Pacific SST still remains many uncertainties. We also inspect the results based on the ERSSTv5 data (Supplementary Fig. 1), and the correlation patterns are consistent, suggesting that the

connection between AMO and CWF seesaw is robust to the choice of SST datasets.

We further examine the relationship of the CWF seesaw with the AMO and PDO, as the spatial correlation patterns exhibit good resemblance to these two climate modes over the North Atlantic and North Pacific basins, respectively. Figure 6 shows the time series of the CWF seesaw, AMO, and PDO index for the period 1900–2019. The CWF seesaw index corresponds well with the AMO index at multidecadal time scales, and the correlation coefficient between them reaches 0.76. The AMO shows turning signs around the 1930 and 1980 s, consistent with the turning signs of the CWF seesaw index. However, the correlation of the CWF seesaw index with the PDO index exhibits less agreement ($r = -0.39$). Before the 1960 s, the two series barely matched, and no significant coherence can be found, indicating that the PDO unlikely plays a role in modulating the CWF seesaw during this period. The CWF seesaw index somehow shows an antiphase relationship with the PDO index since the 1960 s. It is unknown that whether the connection between the PDO and CWF seesaw is strengthening during the recent decades. Nevertheless, the CWF seesaw shows more consistent variation with the AMO, as their phases largely correspond for the overall analyzed period from 1900 to 2019. In this study, we inspect the relationship between the CWF seesaw and the AMO, considering the AMO exhibits a higher correlation with the CWF seesaw over multidecadal time scales.

We further inspect the relationship of the Northern Hemisphere cold wave frequency with the AMO index as well as the CWF seesaw index. In Fig. 7a, the seesaw pattern in CWF is clearly displayed, suggesting that the CWFs in Greenland and central Eurasia are out-of-phase, consistent with the above analysis. It also provides evidence that the seesaw index we defined is capable of representing the spatial features of CWF over the two specified regions. The correlation map between the AMO and CWF exhibits a seesaw

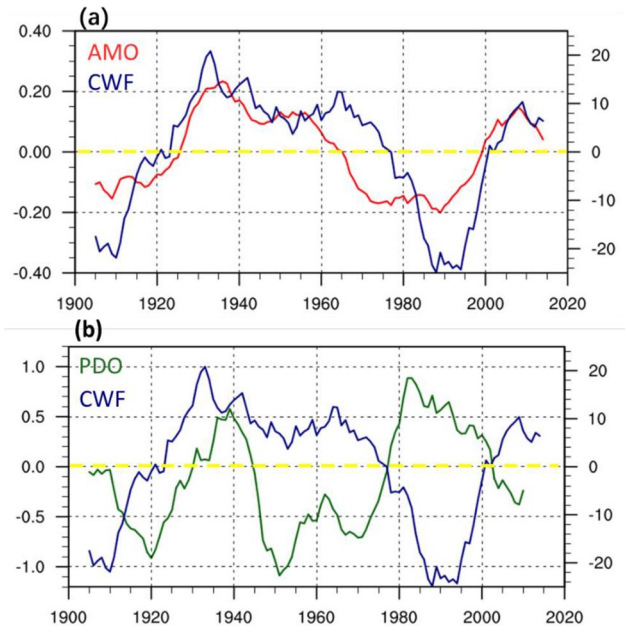

Fig. 6 Time series of 11-year running mean cold wave frequency seesaw index derived from the Berkeley data set for the period 1900–2019 (blue curve; right axis in units of days) and **a** the AMO index (red curve; left axis), **b** the PDO index (green curve; left axis) for the same period. The long-term linear trends were removed. The yellow dash line indicates zero

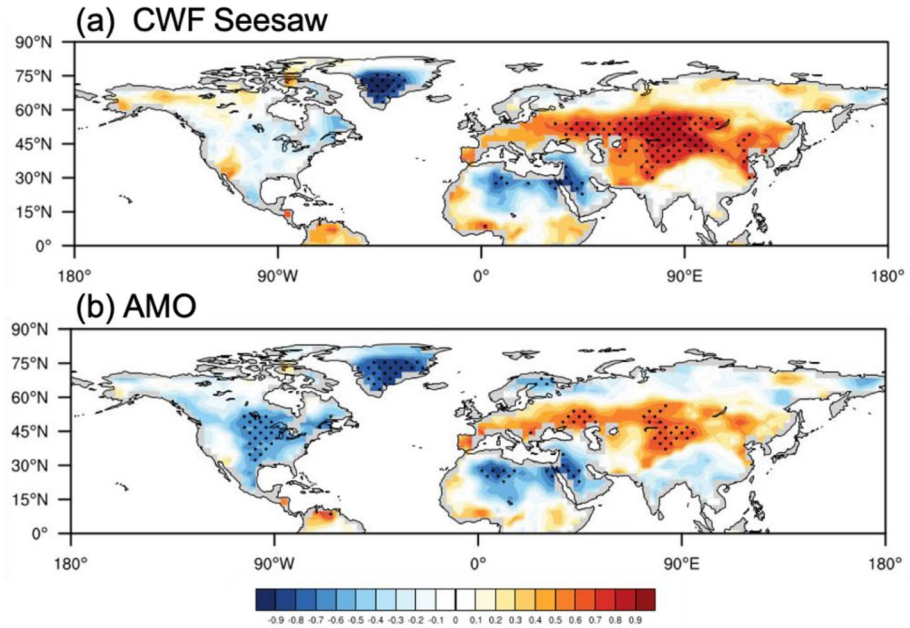

Fig. 7 Correlation maps between cold wave frequency and **a** cold wave frequency seesaw index and **b** AMO index derived from the Berkeley data set for the period 1900–2019. The long-term linear trends were removed before the analysis. Dotted shading indicates the correlation coefficients significant at the 95 % confidence level

pattern as well (Fig. 7b), with a negative correlation over Greenland and a positive correlation over central Eurasia. It indicates that the AMO is closely connected with the CWF decadal variabilities over both regions, further verifying the strong temporal coherence with the CWF seesaw index (Fig. 6a). The spatial patterns are generally consistent between the AMO index and CWF seesaw index, further indicating the existence of the seesaw pattern in CWF, for which the AMO may be responsible.

3.3 Physical mechanism

From the above analysis, the AMO is closely correlated with the CWF seesaw and may play a crucial role in modulating the CWF over central Eurasia and Greenland, but the effects are opposite. In this study, we investigate the possible mechanism of how the AMO influences the CWF seesaw. It is known that changes in mean temperature are closely linked to the frequency of extreme temperatures (Mearns et al. 1984; Meehl et al. 2000). In Fig. 8b, we also inspect the relationship between the CWF seesaw index and the surface air temperature (SAT). The regression map exhibits a seesaw pattern, with a significant cooling over central Eurasia and a significant warming center over Greenland. The correlation patterns of the CWF seesaw index with both CWF (Fig. 7a) and SAT (Fig. 8b) are very alike, indicating that there is a strong coherence between the SAT and CWF. That is, more (less) cold wave frequency corresponds with cooling (warming) in surface air temperature over central Eurasia (Greenland). Here, we inspect the influence of AMO on the Northern Hemisphere surface air temperature (Fig. 8a). Greenland exhibits a strong warming response, while central Eurasia exhibits a cooling response to the AMO, consistent with the seesaw pattern in CWF. The CWF and winter air temperature anomalies consistently show a zonally elongated pattern with pronounced anomalies in central Eurasia related to the AMO (Fig. 8).

To understand how the AMO and the SAT seesaw over Greenland and central Eurasia are connected, we first examine the climatological geopotential heights at 950 hPa. During the wintertime, the Siberian High (SH) is a dominant circulation system that has an influence on the Eurasian continent with excessively low surface air temperature (Panagiotopoulos et al. 2005). Meanwhile, the Icelandic Low (IL) is another semi-permanent low-pressure system, which is recognized to have profound impacts on surface air temperature over Greenland (van Loon and Rogers 1978; Kushnir 1999). Tubi and Dayan (2013) indicate that there is a teleconnection between SH and IL, and the IL may play a dominant role in the variations of SH. During the warm phase of the AMO, the Arctic region exhibits positive anomalies in geopotential heights, resulting in a weakened IL. Over the North Atlantic Ocean, there is a significant dipole pattern in response to the AMO, with an increase in geopotential

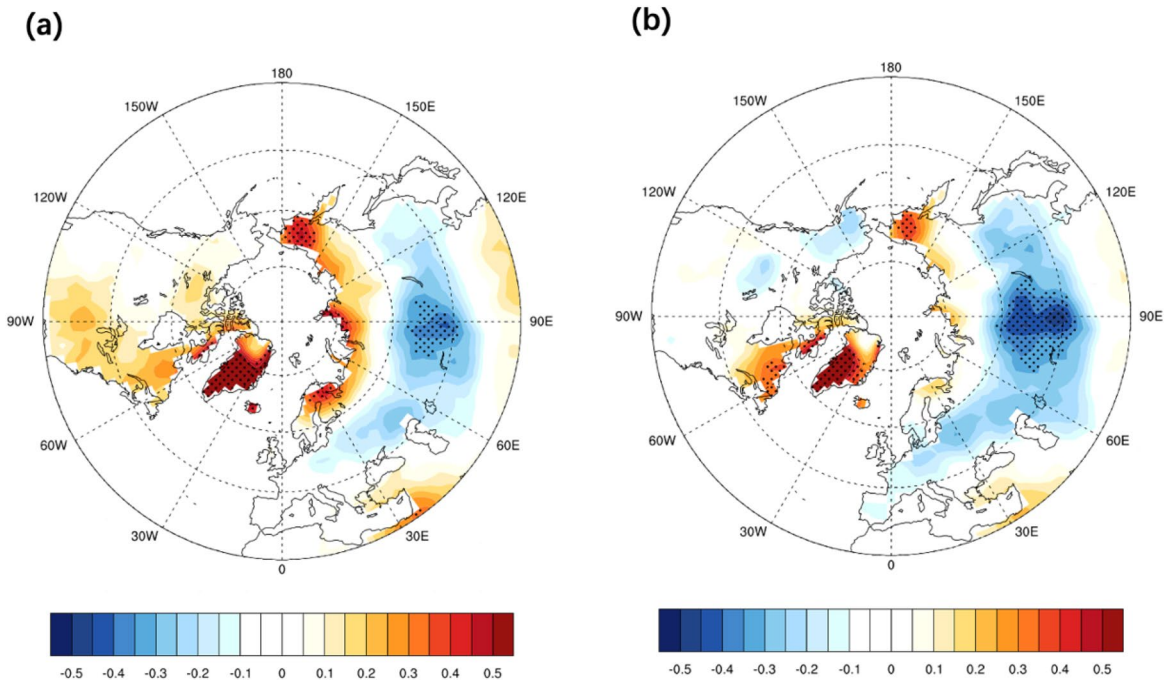

Fig. 8 The regression maps of surface temperatures (units: K) onto the **a** AMO index and **b** cold wave frequency seesaw index derived from the Berkeley data set for the period 1900–2019. The long-term linear trends were removed before the analysis. Dotted shading indicates the correlation coefficients significant at the 95% confidence level

heights over the northern regions (Greenland, Iceland, and the Labrador Sea) and a decline over the subtropical North Atlantic and the Mediterranean Sea. As a result, the weakened IL reduces the northerlies from the polar region due to the smaller-than-normal pressure gradients. With fewer cold advection from higher latitudes, the surface air temperature exhibits a warm anomaly, corresponding to less frequent CW activities. Meanwhile, central Eurasia (especially central Siberia) shows significantly increased geopotential heights in response to the AMO forcing. As suggested in Fig. 9a, the increased geopotential heights over central Eurasia corresponds with the climatological SH, which governs the cold wave activity over central Eurasia. The anomalous geopotential heights over the subpolar region also exhibit a quasi-annular structure corresponding to high-pressure anomalies across mid-high-latitude Eurasia. The continental cold high in Eurasia, including the SH, is enhanced. Consequently, the winter air temperature decreases, corresponding to an increase in CWF.

The zonal averaged atmospheric responses to the AMO forcing are shown in Fig. 10. It suggests that the impacts of AMO not only exist near the surface but also extend to the upper levels. The positive phase of AMO, corresponding to the uniform SST warming over the North Atlantic basin, can exert opposite temperature anomalies over the upper level through an upper-tropospheric anomalous atmospheric circulation response (Ehsan et al. 2020; Nicolì et al. 2020). As shown in Fig. 10a, there is a dipole pattern in air temperature above 300 hPa, with strong upper-level warming over the mid-high latitudes and relatively weak cooling over the subtropical region. The anomalous temperature pattern is caused by the underlying ocean heating in association with the AMO. According to the thermal wind theory, the increased temperature gradients tend to modify the winds. The regression of the wind field onto the AMO index exhibits consistent results (Fig. 10b). There are anomalous easterlies over the upper troposphere, corresponding to the temperature dipole. Consequently, the climatological westerlies are significantly weakened, further resulting in an adjustment in geopotential heights. In Fig. 10c, due to the weakened westerlies, the geopotential height increases over high latitude regions while slightly decreases over the mid-latitude area. Moreover, the geopotential height exhibits consistent uplifts from the upper to lower troposphere near the Arctic. Thus, the AMO induces positive geopotential height anomalies that weaken the IL and strengthen the SH, resulting in a seesaw pattern in surface air temperature. In addition, the increased geopotential height over the Arctic further weakens the upper-level polar vortex. Normally, the Arctic cold air is confined within the polar region due to the polar vortex, and the zonal westerly winds enclose a large pool of extremely cold air. Since the polar vortex is weakened associated with the warm AMO phase, the zonal wind weakens, and the Arctic cold air spills into the mid-latitudes, which leads to more cold air outbreaks and more frequent cold wave events accordingly. This has a profound influence

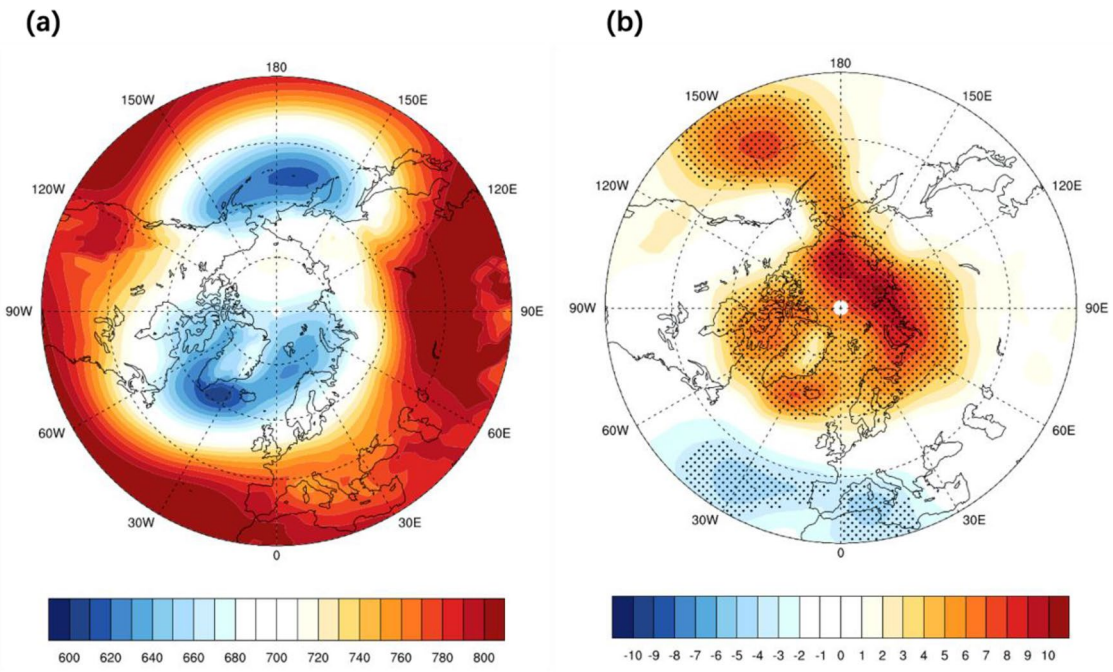

Fig. 9 **a** Climatological geopotential heights at 950 hPa (units: m) from reanalysis data set for the period 1900–2013 and **b** the geopotential heights at 950 hPa regressed onto the AMO index. The long-term linear trends were removed before the analysis. Dotted shading indicates the correlation coefficients significant at the 95% confidence level

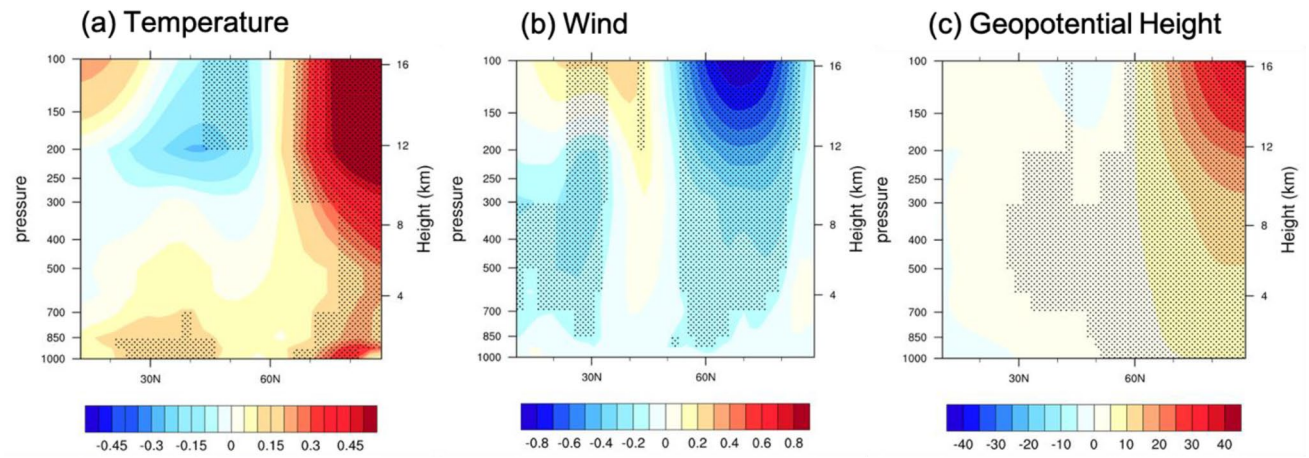

Fig. 10 The zonal averaged **a** air temperatures (units: K), **b** zonal winds (units: m/s), and **c** geopotential heights (units: m) regressed onto the AMO index from reanalysis data set for the period 1900–2013. The long-term linear trends were removed before the analysis. Dotted shading indicates the correlation coefficients significant at the 95 % confidence level

on the CWF in central Eurasia (Huang and Tian 2019; Zhang et al. 2016). Meanwhile, the weakening of zonal westerlies is favorable for warm air from the lower latitudes to move into the higher latitudes, decreasing the CWF over Greenland. The cold AMO phase corresponds to a strengthening of the polar vortex and zonal westerlies, confining the cold air to high latitudes closer to the Arctic and leading to CWF increase in Greenland and decrease in central Eurasia, respectively. We can conclude that the seesaw patterns in SAT and CWF are consistently modulated by the AMO and the associated anomalous atmospheric circulation.

We then conduct the AGCM experiment (NA_EXP) to investigate the influences of AMO on the atmosphere in the numerical model simulation. As shown in Fig. 11a, the model reproduces the surface air temperature seesaw between Greenland and central Eurasia, and the spatial

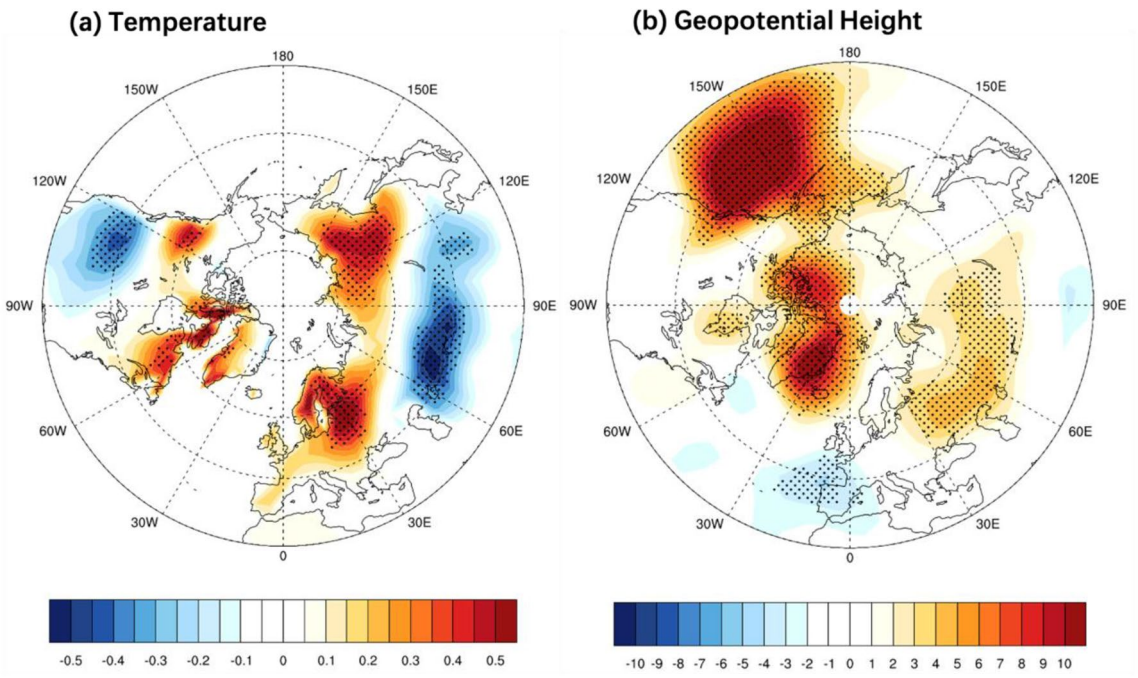

Fig. 11 The **a** surface air temperatures (units: K) and **b** geopotential heights at 925 hPa (units: m) regressed on the AMO index in NA_EXP AGCM simulation for the period 1900–2013. The long-term linear trends were removed before the analysis. Dotted shading indicates the correlation coefficients significant at the 95 % confidence level

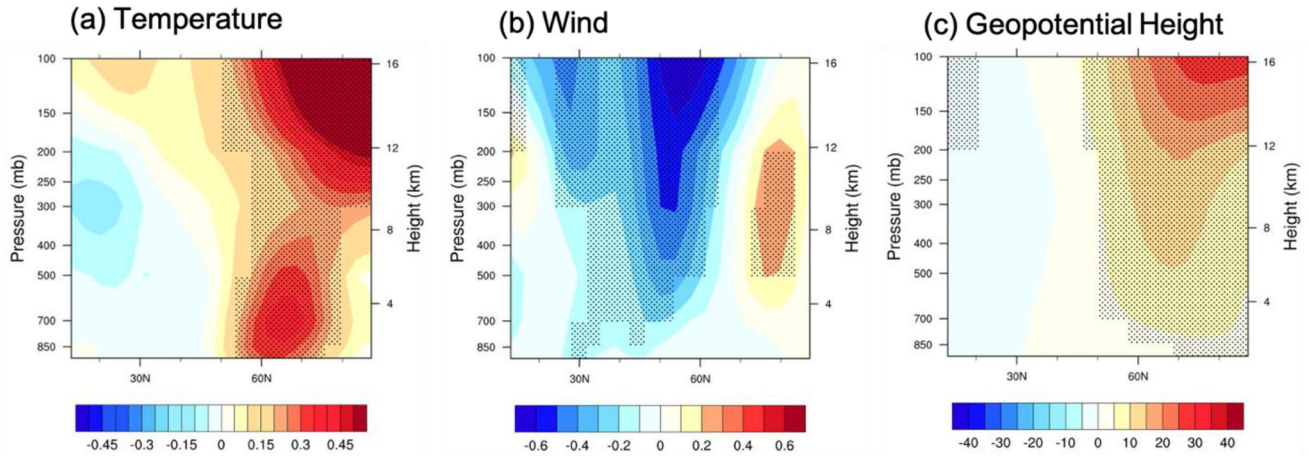

Fig. 12 The zonal averaged **a** air temperatures (units: K), **b** zonal winds (units: m/s), and **c** geopotential heights (units: m) regressed on the AMO index in NA_EXP AGCM simulation for the period 1900–2013. The long-term linear trends were removed before the analysis. Dotted shading indicates the correlation coefficients significant at the 95 % confidence level

regression pattern is overall consistent with that observed in Fig. 8a. It provides model evidence that the AMO is critical in the formation of the surface air temperature\CWF seesaw. Moreover, the model simulates an annular-like regression pattern, with strong warming responses over the Pan-Artic regions and cooling responses over lower-latitude regions. However, there are still some biases. For example, the model overestimates the responses over northern Europe and eastern Siberia, and North American cooling is not observed. The simulated responses of 950 hPa geopotential height (Fig. 11b) also show good agreement with the observed pattern. The mid-high latitude regions exhibit a significant increase in geopotential heights, corresponding to a weakened IL and strengthened SH. Thus, model simulation suggests that the changes in surface air temperature are directly influenced by the anomalous near-surface pressure systems, which are further modulated by the AMO, consistent with the observations.

We also inspect the upper-level tropospheric responses to the AMO in NA_EXP (Fig. 12). Due to the AMO-induced North Atlantic warming, the upper-level atmosphere is significantly heated by the underlying ocean, exhibiting a strong warming pattern as shown in the observation. Although the dipole pattern is not fully reproduced, the increased temperature gradients are also significant in the model simulation. The anomalous meridional thermal differences induce strong easterlies that offset the predominant westerlies, resulting in a geostrophic adjustment in geopotential heights. Note that the location of the weakened westerlies exhibits a slight southward shift, which could be related to the model performance of ICTPAGCM in simulating the jet stream (Kucharski et al. 2013). Nevertheless, the anomalously high geopotential heights are found north of 60° N in response to the weakened westerlies, which further leads to the high-pressure anomalies near the surface, consistent with the observations. The NA_EXP successfully reproduces the critical processes that the AMO induces upper troposphere warming and the associated upraise in geopotential heights over the Arctic, which further modulates the surface air temperature, resulting in Greenland warming and central Eurasia cooling. The upper-level atmospheric circulation changes result in a weakened polar vortex and consequently a seesaw in CWF over Greenland and central Eurasia, corresponding to the surface air temperature.

As shown in Figs. 5b and 6b, there is coherence between the CWF and the PDO, but only since the 1950 s. To better evaluate the role of the PDO, we perform further analysis using the Berkeley dataset from 1950 to 2019 since the coherence is relatively stronger during this period. We first inspect the correlation between the CWF and the PDO index (Supplementary Fig. 2). The CWF in central Eurasia and the PDO are significantly correlated. However, although the CWF in Greenland is negatively correlated with the PDO index, the correlation coefficients are rather weak and insignificant, indicating that the influence of PDO on the Greenland CWF is very limited. Consequently, the seesaw feature in the spatial pattern of PDO-related CWF is rather weak in comparison with the observed seesaw pattern in Fig. 7a. Therefore, we can infer that the coherence between the PDO and the CWF seesaw index after the 1950 s may be more related to the central Eurasia CWF counterpart. By contrast, the AMO-related CWF responses are prominent in both Greenland and central Eurasia, indicating that the AMO may play a more important role in the CWF seesaw than the PDO. We further inspect the upper-level atmospheric circulation responses to the PDO (Supplementary Fig. 3). The negative PDO phase can induce upper-level air temperature warming in high-latitude and weaken the subpolar

westerly jet and polar vortex, which may explain the coherence between the PDO and central Eurasian cold wave activity. A previous study suggested that the negative PDO tends to weaken the Aleutian Low and further reduces the jet stream over the subpolar North Pacific, contributing to the changes in zonal mean atmospheric circulation (Hu and Guan 2018). Despite that the regression patterns associated with the PDO bear some resemblance to those related to the AMO, the underlying mechanism may be distinguished, and the atmospheric responses to the PDO are relatively weaker than to the AMO (Fig. 10). This evidence suggests that the PDO unlikely plays a dominant role since its influence is mainly confined over the Eurasian continent and the North Pacific. We also inspect the partial correlation between the CWF and AMO with the PDO signal removed for the whole analysis period 1900–2019 (Supplementary Fig. 4), and the seesaw pattern is still prominent and consistent with that in Fig. 7b. The above analysis indicates that the influence of AMO on the CWF seesaw and corresponding atmospheric circulation is stronger than the PDO, and the connection between CWF seesaw and AMO is prominent throughout the whole analysis period since 1900 and independent of the PDO signal.

4 Summary and discussion

The cold wave is an important extreme weather event and is commonly seen in the Northern Hemisphere winter. It causes great social and economic damage every year, threatening the wellbeing of those people who live in the mid-high latitude regions. The cold wave frequency (CWF) exhibits contrasting long-term trends over Greenland and central Eurasia, implying a potential linkage between them. Other than the long-term trend, the CWF also exhibits significant multidecadal variability. In this study, we find that the CWFs between Greenland and central Eurasia exhibit an out-of-phase relationship ($r = -0.70$), referring to as the multidecadal seesaw. The CWF seesaw strongly correlates with the Northern Hemisphere SSTs, especially over the North Atlantic. It is suggested that the positive phase of AMO induces upper-level troposphere warming over the mid-high latitudes and cooling over the subtropical area. The increased temperature gradients significantly weaken the westerlies over the Arctic and lead to the uplift of geopotential heights over high latitudes troposphere. It corresponds with the increase in the lower level pressure that weakens the Icelandic Low and strengthens the Siberian High, resulting in the Greenland warming and central Eurasia cooling. The AMO-induced geopotential height increases also lead to a weakened polar vortex, which leads to more (less) frequent cold wave frequency over central Eurasia (Greenland). Moreover, the NA_EXP, which only takes the North Atlantic SST into consideration, successfully reproduces the observed seesaw pattern and the physical mechanism are also well displayed. Thus, we may conclude that the CWF seesaw over Greenland and central Eurasia is robust on multidecadal time scales and the AMO plays a forcing role in its formation.

In this study, we also compare the relative role of Arctic sea ice and SST modes in forcing the CWF seesaw. It is suggested that the variability of Arctic sea ice does not correspond with the CWF seesaw very well ($r = -0.17$) for the whole analysis period since 1900, indicating that the CWF seesaw is unlikely dominated by the sea ice forcing. Despite the weak correlation of CWF seesaw with the whole Arctic sea ice, there is coherence between the CWF seesaw and regional sea ice around Greenland. Previous studies demonstrated that the AMO also contributes to the low-frequency variability of the Arctic sea ice (Day et al. 2012; Mahajan et al. 2011; Miles et al. 2014; Zhang 2015). Thus, the connection between the regional sea ice and the CWF seesaw may be related to the AMO to some extent, which needs further inspection. It is also worth noticing that recent studies suggested a potential impact of the North Atlantic on the North Pacific SST, especially during the recent decades (Li et al. 2016; Kucharski et al. 2016a, b; Zhang and Delworth 2007). Considering the connection of decadal SST variations between these two ocean basins, the relationship between the PDO and zonal mean circulation and hence the CWF may have contributions from the North Atlantic Ocean. How to quantitatively distinguish the relative influence of PDO and AMO on the zonal mean atmospheric anomalies requires future investigation.

Supplementary Information The online version contains supplementary material available at https://doi.org/10.1007/s00382-021-05967-7.

Acknowledgements The authors wish to thank the anonymous reviewers for their constructive comments that significantly improved the quality of this paper. This work was jointly supported by the National Natural Science Foundation of China (41790474, 41775038 and 41975082), Shandong Natural Science Foundation Project (ZR2019ZD12) and the National Programme on Global Change and Air–Sea Interaction (GASI-IPOVAI-06 and GASI-IPOVAI-03).

Data availability All data generated or analysed during this study are included in this published article.

References

Anandhi A, Hutchinson S, Harrington J, Rahmani V, Kirkham MB, Rice CW (2016) Changes in spatial and temporal trends in wet, dry, warm and cold spell length or duration indices in Kansas, USA. Int J Climatol 36:4085–4101

Barnes EA, Dunn-Sigouin E, Masato G, Woollings T (2014) Exploring recent trends in Northern Hemisphere blocking. Geophys Res Lett 41:638–644

Caesar J, Alexander L, Vose R (2006) Large-scale changes in observed daily maximum and minimum temperatures: creation and analysis of a new gridded data set. J Geophys Res 111:D05101

Chen S, Song L, Chen W (2019) Interdecadal modulation of AMO on the winter North Pacific Oscillation-following winter ENSO relationship. Adv Atmos Sci 36:1393–1403. https://doi.org/10.1007/s00376-019-9090-1

Cohen J (2016) An observational analysis: tropical relative to Arctic influence on midlatitude weather in the era of Arctic amplification. Geophys Res Lett 43:5287–5529

Cohen JL, Furtado JC, Barlow MA, Alexeev VA, Cherry JE (2012) Arctic warming, increasing snow cover and widespread boreal winter cooling. Environ Res Lett 7:014007

Compo GP et al (2011) The twentieth century reanalysis project. QJR Meteorol Soc 137:1–28

Day JJ, Hargreaves JC, Annan JD, Abe-Ouchi A (2012) Sources of multi-decadal variability in Arctic sea ice extent. Environ Res Lett. https://doi.org/10.1088/1748-9326/7/3/034011

Ding QH, Wallace JM, Battisti DS, Steig EJ, Gallant AJE, Kim HJ, Geng L (2014) Tropical forcing of the recent rapid Arctic warming in northeastern Canada and Greenland. Nature 509(7499):209–212

Ding Q et al. (2019) Fingerprints of internal drivers of Arctic sea ice loss in observations and model simulations. Nat Geosci 12:28

Ehsan MA, Nicolì D, Kucharski F et al (2020) Atlantic Ocean influence on Middle East summer surface air temperature. npj Clim Atmos Sci 3:5. https://doi.org/10.1038/s41612-020-0109-1

Enfield DB, Mestas-Nuñez AM, Trimble PJ (2001) The Atlantic multidecadal oscillation and its relation to rainfall and river flows in the continental US. Geophys Res Lett 28:2077–2080

Feng S, Hu Q, Oglesby RJ (2011) Influence of Atlantic sea surface temperatures on persistent drought in North America. Clim Dyn 37:569–586

Francis JA, Vavrus SJ (2012) Evidence linking Arctic amplification to extreme weather in mid-latitudes. Geophys Res Lett 39:L06801

Francis JA, Vavrus SJ (2015) Evidence for a wavier jet stream in response to rapid Arctic warming. Environ Res Lett 10:014005

Gao YQ et al (2015) Arctic sea ice and Eurasian climate: a review. Adv Atmos Sci 32:92–114

Gong DY, Wang SW, Zhu JH (2001) East Asian winter monsoon and Arctic oscillation. Geophys Res Lett 28:2073–2076

Gong Z et al (2020) An inter-basin teleconnection from the North Atlantic to the subarctic North Pacific at multidecadal time scales. Clim Dyn 54:807–822

Griffiths GM, Chambers LE, Haylock MR, Manton MJ, Nicholls N, Baek HJ, Choi Y, Della-Marta PM, Gosai A, Iga N, Lata R, Laurent V, Maitrepierre L, Nakamigawa H, Ouprasitwong N, Solofa D, Tahani L, Thuy DT, Tibig L, Trewin B, Vediapan K, Zhai P (2005) Change in mean temperature as a predictor of extreme temperature change in the Asia–Pacific region. Int J Climatol 25(10):1301–1330

Harris I, Jones PD, Osborn TJ, Lister DH (2013) Updated high-resolution grids of monthly climatic observations. In press. Int J Climatol. Doi:https://doi.org/10.1002/joc.3711

Honda M, Inoue J, Yamane S (2009) Influence of low Arctic sea-ice minima on anomalously cold Eurasian winters. Geophys Res Lett. https://doi.org/10.1029/2008GL037079

Horton DE, Johnson NC, Singh D, Swain DL, Rajaratnam B, Diffenbaugh NS (2015) Contribution of changes in atmospheric circulation patterns to extreme temperature trends. Nature 522(7557):465–469

Hu DZ, Guan ZY (2018) Decadal Relationship between the Stratospheric Arctic Vortex and Pacific Decadal. Oscil J Clim 31:3371–3386. https://doi.org/10.1175/jcli-d-17-0266.1

Huang JL, Tian WS (2019) Eurasian cold air outbreaks under different arctic stratospheric polar vortex strengths. J Atmos Sci 76:1245–1264. https://doi.org/10.1175/jas-d-18-0285.1

Huang B et al (2017a) NOAA extended reconstructed sea surface temperature (ERSST), version 5. NOAA Natl Cent Environ Inf 30:8179–8205

Huang J, Xie Y, Guan X, Guan D, Li, Ji F (2017b) The dynamics of the warming hiatus over the Northern Hemisphere. Clim Dyn 48:429–446

Jia X, Ge J (2017) Interdecadal changes in the relationship between ENSO, EAWM, and the wintertime precipitation over China at the end of the twentieth century. J Clim 30:1923–1937

Jiang XW, Yang S, Li Y, Kumar A, Wang W, Gao Z (2013) Dynamical prediction of the East Asian winter monsoon by the NCEP Climate Forecast System. J Geophys Res Atmos 118:1312–1328

Jung O, Sung M-K, Sato K, Lim Y-K, Kim S-J, Baek E-H, Jeong J-H, Kim B-M (2017) How does the SST variability over the western North Atlantic Ocean control Arctic warming over the Barents–Kara Seas? Environ Res Lett 12(3):034021

Karl TR, Knight RW, Plummer N (1995) Trends in high-frequency climate variability in the twentieth century. Nature 377:217–220

Kelleher M, Screen J (2018) Atmospheric precursors of and response to anomalous Arctic sea ice in CMIP5 models. Adv Atmos Sci 35:27–37

Kerr RA (2000) A North Atlantic climate pacemaker for the centuries. Science 288:1984–1986

Kucharski F, Molteni F, King MP, Farneti R, Kang I-S, Feudale L (2013) On the need of intermediate complexity general circulation models a "SPEEDY". Ex Bull Am Meteorol Soc 94:25–30. https://doi.org/10.1175/bams-d-11-00238.1

Kucharski F et al (2016a) Atlantic forcing of Pacific decadal variability. Clim Dyn 46:2337–2351. doi:https://doi.org/10.1007/s00382-015-2705-z

Kucharski F, Parvin A, Rodriguez-Fonseca B, Farneti R, Martin-Rey M, Polo I et al (2016b) The teleconnection of the tropical Atlantic to Indo-Pacific sea surface temperatures on inter-annual to centennial time scales: a review of recent findings. Atmosphere 7(2):29. doi:10.3390/atmos7020029

Kug J-S, Jeong J-H, Jang Y-S, Kim B-M, Folland CK, Min S-K, Son S-W (2015) Two distinct influences of Arctic warming on cold winters over North America and East Asia. Nat Geosci 8:759

Kushnir Y (1999) Europe's winter prospects. Nature 398:289–291. https://doi.org/10.1038/18560

Li S, Bates GT (2007) Influence of the Atlantic multidecadal oscillation on the winter climate of East China. Adv Atmos Sci 24:126–135

Li J, Sun C, Jin FF (2013) NAO implicated as a predictor of Northern Hemisphere mean temperature multidecadal variability. Geophys Res Lett 40:5497–5502

Li C, Stevens B, Marotzke J (2015) Eurasian winter cooling in the warming hiatus of 1998–2012. Geophys Res Lett 42:8131–8139

Li X, Xie S-P, Gille ST, Yoo C (2016) Atlantic-induced pan-tropical climate change over the past three decades. Nat Clim Change 6:275–279

Li F, Orsolini YJ, Wang HJ, Gao YQ, He SP (2018) Atlantic multidecadal oscillation modulates the impacts of Arctic sea ice decline. Geophys Res Lett 45:2497–2506

Li J, Zheng F, Sun C, Feng J, Wang J (2019a) Pathways of influence of the Northern Hemisphere mid-high latitudes on East Asian climate: a review. Adv Atmos Sci 36(9):902–921

Li X, Wu Z, Li Y (2019b) A link of China warming hiatus with the winter sea ice loss in Barents–Kara Seas. Clim Dyn 53:2625–2642. https://doi.org/10.1007/s00382-019-04645-z

Liu J, Curry JA, Wang H, Song M, Horton RM (2012) Impact of declining Arctic sea ice on winter snowfall. Proc Natl Acad Sci 109:4074–4079

Lu R, Dong B, Ding H (2006) Impact of the Atlantic Multidecadal Oscillation on the Asian summer monsoon. Geophys Res Lett. https://doi.org/10.1029/2006GL027655

Luo Y, Chen A, Dai M, Mu R, Zhang, Ian S (2017) Winter Eurasian cooling linked with the Atlantic multidecadal oscillation. Environ Res Lett 12:125002

Ma SM, Zhu CW (2019) Extreme cold wave over East Asia in January 2016: a possible response to the larger internal atmospheric variability induced by Arctic warming. J Clim 32:1203–1216

Ma SM, Zhu CW, Liu BQ, Zhou TJ, Ding YH, Orsolini YJ (2018) Polarized response of east asian winter temperature extremes in the era of arctic warming. J Clim 31(14):5543–5557

Mahajan S, Zhang R, Delworth TL (2011) Impact of the Atlantic Meridional Overturning Circulation (AMOC) on Arctic surface air temperature and sea ice. Var J Clim 24:6573–6581. https://doi.org/10.1175/2011jcli4002.1

Mantua NJ, Hare SR, Zhang Y, Wallace JM, Francis RC (1997) A Pacific interdecadal climate oscillation with impacts on salmon production. Bull Am Meteorol Soc 78:1069–1080

McCabe GJ, Palecki MA, Betancourt JL (2004) Pacific and Atlantic Ocean influences on multidecadal drought frequency in the United States. Proc Natl Acad Sci 101:4136–4141

Mearns LO, Katz RW, Schneider SH (1984) Extreme high-temperature events: changes in their probabilities with changes in mean temperature. J Appl Meteorol 23:1601–1613

Meehl GA, Karl T, Easterling DR, Changnon S, Pielke R Jr, Changnon D, Evans J, Groisman PY, Knutson TR, Kunkel KE, Mearns LO, Parmesan C, Pulwarty R, Root T, Sylves RT, Whetton P, Zwiers F (2000) An introduction to trends in extreme weather and climate events: observations, socio-economic impacts, terrestrial ecological impacts, and model projections. Bull Am Meteorol Soc 81(3):413–416

Miles MW, Divine DV, Furevik T, Jansen E, Moros M, Ogilvie AEJ (2014) A signal of persistent Atlantic multidecadal variability in Arctic sea ice. Geophys Res Lett 41:463–469. doi:https://doi.org/10.1002/2013gl058084

Mori M, Watanabe M, Shiogama H, Inoue J, Kimoto M (2014) Robust Arctic sea-ice influence on the frequent Eurasian cold winters in past decades. Nat Geosci 7:869–873

Nairn J, Fawcett R (2013) Defining heatwaves: heatwave defined as a heat-impact event servicing all community and business sectors in Australia. Technical Report No. 60. The Centre for Australian Weather and Climate Research, Melbourne, Australia

Nairn JR, Fawcett RJB (2015) The excess heat factor: a metric for heatwave intensity and its use in classifying heatwave severity. Int J Environ Res Public Health 12:227–253

Nicolì D, Bellucci A, Iovino D et al (2020) The impact of the AMV on Eurasian summer hydrological cycle. Sci Rep 10:14444

O'Reilly CH, Woollings T, Zanna L (2017) The dynamical influence of the Atlantic Multidecadal Oscillation on continental climate. J Clim 30(18):7213–7230

Outten SD, Esau I (2012) A link between Arctic sea ice and recent cooling trends over Eurasia. Clim Change 110:1069–1075

Overland J, Francis JA, Hall R, Hanna E, Kim S-J, Vihma T (2015) The melting Arctic and midlatitude weather patterns: are they connected? J Clim 28(20):7917–32

Panagiotopoulos F, Shagedanova M, Hannachi A, Stephenson D (2005) Observed trends and teleconnections of the Siberian High: a recently declining center of action. J Clim 18(9):1411–1422

Perlwitz J, Hoerling M, Dole R (2015) Arctic tropospheric warming: causes and linkages to lower latitudes. J Clim 28(6):2154–2167

Piticar A, Croitoru AE, Ciupertea FA, Harpa GV (2018) Recent changes in heat waves and cold waves detected based on excess heat factor and excess cold factor in Romania. Int J Climatol 38:1777–1793

Rhines A, McKinnon KA, Tingley MP, Huybers P (2017) Seasonally resolved distributional trends of North Amer- ican temperatures show contraction of winter variability. J Clim 30:1139–1157

Rohde RA, Hausfather Z (2020) The Berkeley earth land/ocean temperature record. Earth Syst Sci Data 12:34693479

Scalley BD, Spicer T, Jian L, Xiao J, Nairn J, Robertson A, Weeramanthri T (2015) Responding to heatwaves intensity: excess heat factor is a superior predictor of health service utilisation and a trigger for heatwaves plans. Aust NZ J Public Health 39:582–587

Schweiger AJ, Wood KR, Zhang J (2019) Arctic sea ice volume variability over 1901–2010: a model-based reconstruction. J Clim 32:4731–4752

Screen JA (2014) Arctic amplification decreases temperature variance in northern mid- to high-latitudes. Nat Clim Change 4:577–582

Screen JA (2017) The missing Northern European winter cooling response to Arctic sea ice loss. Nat Commun 8:14603

Screen JA, Simmonds I (2010) The central role of diminishing sea ice in recent Arctic temperature amplification. Nature 464:1334

Screen JA, Deser C, Simmonds I (2012) Local and remote controls on observed Arctic warming. Geophys Res Lett. https://doi.org/10.1029/2012GL051598

Screen JA, Deser C, Sun LT (2015) Reduced risk of North American cold extremes due to continued Arctic sea ice loss. Bull Am Meteorol Soc 96(9):1489–1503

Screen JA, Simmonds I, Deser C, Tomas R (2013) The atmospheric response to three decades of observed Arctic sea ice loss. J Clim 26:1230–1248

Sen PK (1968) Estimates of the regression coefficient based on Kendall's tau. J Am Stat Assoc 63(324):1379–1389

Serreze MC, Barry RG (2011) Processes and impacts of Arctic amplification: a research synthesis. Glob Planet Change 77:85–96

Sigmond M, Fyfe JC (2016) Tropical Pacific impacts on cooling North American winters. Nat Clim Change 6(10):970–974

Smith TM, Reynolds RW, Peterson TC, Lawrimore J (2008) Improvements to NOAA's historical merged land–ocean surface temperature analysis (1880–2006). J Clim 21:2283–2296

Spinoni J, Lakatos M, Szentimrey T, Bihari Z, Szalai S, Vogt J, Antofie T (2015) Heat and cold waves trends in Carpathian region from 1961 to 2010. Int J Clim 35:4197–4209

Sun C, Li J, Zhao S (2015) Remote influence of Atlantic multidecadal variability on Siberian warm season precipitation. Sci Rep 5:16853

Sun C, Li JP, Ding RQ (2016a) Strengthening relationship between ENSO and western Russian summer surface temperature. Geophys Res Lett 43:843–851

Sun CH, Yang S, Li W, Zhang R, Wu R (2016b) Interannual variations of the dominant modes of East Asian winter monsoon and possible links to Arctic sea ice. Clim Dyn 47:481–496

Sun L, Perlwitz J, Hoerling M (2016c) What caused the recent "Warm Arctic, Cold Continents" trend pattern in winter temperatures? Geophys Res Lett 43:5345–5352

Sun C, Kucharski F, Li J, Jin FF, Kang IS, Ding R (2017a) Western tropical Pacific multidecadal variability forced by the Atlantic multidecadal oscillation. Nat Commun 8:15998

Sun C, Li JP, Ding RQ, Jin Z (2017b) Cold season Africa–Asia multidecadal teleconnection pattern and its relation to the Atlantic multidecadal variability. Clim Dyn 48:3903–3918

Sun C, Kucharski F, Li J, Wang K, Kang IS, Lian T et al (2019) Spring Aleutian Low weakening and surface cooling trend in northwest North America during recent decades. J Geophys Res Atmos 124:078–012,092

Sutton RT, Dong B (2012) Atlantic Ocean influence on a shift in European climate in the 1990s. Nat Geosci 5:788–792
Sutton RT, Hodson DL (2005) Atlantic Ocean forcing of North American and European summer climate. Science 309:115–118
Tokinaga H, Xie SP, Mukougawa H (2017) Early 20th-century Arctic warming intensified by Pacific and Atlantic multidecadal variability. Proc Natl Acad Sci USA 114(24):6227–6232
Tubi A, Dayan U (2013) The Siberian High: teleconnections, extremes and association with the Icelandic Low. Int J Climatol 33:1357–1366. https://doi.org/10.1002/joc.3517
van Loon H, Rogers JC (1978) The seesaw in winter temperatures between Greenland and Northern Europe. Part I: General description. Mon Weather Rev 106:296–310
Wang L, Chen W (2014) An intensity index for the East Asian winter monsoon. J Clim 27:2361–2374
Wang L, Huang R, Gu L, Chen W, Kang L (2009) Interdecadal variations of the East Asian winter monsoon and their association with quasi-stationary planetary wave activity. J Clim 22:4860–4872
Wang Y, Shi L, Zanobetti A, Schwartz JD (2016) Estimating and projecting the effect of cold waves on mortality in 209 US cities. Environ Int 94:141–149
Wang L, Liu Y, Zhang Y, Chen W, Chen SF (2019) Time-varying structure of the wintertime Eurasian pattern: role of the North Atlantic sea surface temperature and atmospheric mean flow. Clim Dyn 52:2467–2479
Wu B, Wang J (2002a) Winter Arctic oscillation, Siberian high and East Asian winter monsoon. Geophys Res Lett 29:3
Wu B, Wang J (2002b) Possible impacts of winter Arctic Oscillation on Siberian high, the East Asian winter monsoon and sea–ice extent. Adv Atmos Sci 19:297–320
Wu Z, Li J, Wang B, Liu X (2009) Can the Southern Hemisphere annular mode affect China winter monsoon? J Geophys Res 114:D11107. doi:https://doi.org/10.1029/2008JD011501
Yu B, Lin H (2018) Coherent changes of wintertime surface air temperatures over North Asia and North America. Sci Rep 8:1–7
Zhang R (2015) Mechanisms for low-frequency variability of summer Arctic sea ice extent. Proc Natl Acad Sci USA 112:4570–4575. https://doi.org/10.1073/pnas.1422296112
Zhang R, Delworth TL (2007) Impact of the Atlantic Multidecadal Oscillation on North Pacific climate variability. Geophys Res Lett. https://doi.org/10.1029/2007gl031601
Zhang XD, Lu CH, Guan ZY (2012) Weakened cyclones, intensified anticyclones and recent extreme cold winter weather events in Eurasia. Environ Res Lett 7(4):044044
Zhang J, Tian W, Chipperfield MP, Xie F, Huang J (2016) Persistent shift of the Arctic polar vortex towards the Eurasian continent in recent decades. Nat Clim Change 6:1094–1099
Zhao S, Li J, Sun C (2016) Decadal variability in the occurrence of wintertime haze in central eastern China tied to the Pacific Decadal Oscillation. Sci Rep 6(1):27424